molecules

MDPI

Review

Noble-Gas Chemistry More than Half a Century after the First Report of the Noble-Gas Compound

Zoran Mazej

Department of Inorganic Chemistry and Technology, Jožef Stefan Institute, Jamova cesta 39, SI–1000 Ljubljana, Slovenia; zoran.mazej@ijs.si; Tel.: +386-1-477-3301

Academic Editor: Felice Grandinetti
Received: 8 June 2020; Accepted: 30 June 2020; Published: 1 July 2020

Abstract: Recent development in the synthesis and characterization of noble-gas compounds is reviewed, i.e., noble-gas chemistry reported in the last five years with emphasis on the publications issued after 2017. XeF_2 is commercially available and has a wider practical application both in the laboratory use and in the industry. As a ligand it can coordinate to metal centers resulting in $[M(XeF_2)_x]^{n+}$ salts. With strong Lewis acids, XeF_2 acts as a fluoride ion donor forming $[XeF]^+$ or $[Xe_2F_3]^+$ salts. Latest examples are $[Xe_2F_3][RuF_6]\cdot XeF_2$, $[Xe_2F_3][RuF_6]$ and $[Xe_2F_3][IrF_6]$. Adducts $NgF_2\cdot CrOF_4$ and $NgF_2\cdot 2CrOF_4$ (Ng = Xe, Kr) were synthesized and structurally characterized at low temperatures. The geometry of XeF_6 was studied in solid argon and neon matrices. Xenon hexafluoride is a well-known fluoride ion donor forming various $[XeF_5]^+$ and $[Xe_2F_{11}]^+$ salts. A large number of crystal structures of previously known or new $[XeF_5]^+$ and $[Xe_2F_{11}]^+$ salts were reported, i.e., $[Xe_2F_{11}][SbF_6]$, $[XeF_5][SbF_6]$, $[XeF_5][Sb_2F_{11}]$, $[XeF_5][BF_4]$, $[XeF_5][TiF_5]$, $[XeF_5]_5[Ti_{10}F_{45}]$, $[XeF_5][Ti_3F_{13}]$, $[XeF_5]_2[MnF_6]$, $[XeF_5][MnF_5]$, $[XeF_5]_4[Mn_8F_{36}]$, $[Xe_2F_{11}]_2[SnF_6]$, $[Xe_2F_{11}]_2[PbF_6]$, $[XeF_5]_4[Sn_5F_{24}]$, $[XeF_5][Xe_2F_{11}][Cr^{V}OF_5]\cdot 2Cr^{VI}OF_4$, $[XeF_5]_2[Cr^{IV}F_6]\cdot 2Cr^{VI}OF_4$, $[Xe_2F_{11}]_2[Cr^{IV}F_6]$, $[XeF_5]_2[Cr^{V}{}_2O_2F_8]$, $[XeF_5]_2[Cr^{V}{}_2O_2F_8]\cdot 2HF$, $[XeF_5]_2[Cr^{V}{}_2O_2F_8]\cdot 2XeOF_4$, $A[XeF_5][SbF_6]_2$ (A = Rb, Cs), $Cs[XeF_5][Bi_xSb_{1-x}F_6]_2$ (x = ~0.37–0.39), $NO_2XeF_5(SbF_6)_2$, $XeF_5M(SbF_6)_3$ (M = Ni, Mg, Zn, Co, Cu, Mn and Pd) and $(XeF_5)_3[Hg(HF)]_2(SbF_6)_7$. Despite its extreme sensitivity, many new XeO_3 adducts were synthesized, i.e., the 15-crown adduct of XeO_3, adducts of XeO_3 with triphenylphosphine oxide, dimethylsulfoxide and pyridine-N-oxide, and adducts between XeO_3 and N-bases (pyridine and 4-dimethylaminopyridine). $[Hg(KrF_2)_8][AsF_6]_2\cdot 2HF$ is a new example of a compound in which KrF_2 serves as a ligand. Numerous new charged species of noble gases were reported ($ArCH_2{}^+$, $ArOH^+$, $[ArB_3O_4]^+$, $[ArB_3O_5]^+$, $[ArB_4O_6]^+$, $[ArB_5O_7]^+$, $[B_{12}(CN)_{11}Ne]^-$). Molecular ion HeH^+ was finally detected in interstellar space. The discoveries of Na_2He and ArNi at high pressure were reported. Bonding motifs in noble-gas compounds are briefly commented on in the last paragraph of this review.

Keywords: helium; neon; argon; krypton; xenon; noble gases; fluorides; oxides

1. Introduction

After almost 20 years, when the Christe's paper "A renaissance in noble gas chemistry" appeared [1], we can say that the renaissance still lasts, although to a lesser extent than in the past. Times are changing, and with that, the fields of research in science. However, new topics are also present in noble-gas (Ng) chemistry. Beside classical Ng chemistry, which includes the syntheses of larger quantities of noble gas compounds (bulk-phase compounds), nowadays there are many other kinds of studies connected with the identification and characterization of molecules of Ng compounds. They include the preparations of Ng compounds in cold matrices, syntheses in liquid and supercritical noble gases, formations of Ng compounds under high pressures, and syntheses of neutral and gas-ion compounds in the gas phase [2]. Lastly, we should not forget to mention a large number of theoretical papers predicting new Ng compounds, which still need to be experimentally confirmed.

The last extensive review of Ng compounds was published in 2018 [2]. It gives a short overview of bulk-phase compounds, molecules of Ng compounds formed in cold matrices, molecules formed in liquid and supercritical noble gases, and the formation of Ng compounds under high pressures. Chapters that are more extensive are related to theoretical chemistry and to gas-phase chemistry of the noble gases. Before that reviews were given by Haner and Schrobilgen in 2015 (xenon(IV) compounds) [3], Nabiev et al. in 2014 (structures of Ng compounds) [4], Brock et al. in 2013 (general about Ng compounds) [5], and Hope in 2013 (coordination chemistry of Ng compounds) [6]. An extensive list of older references of Ng chemistry reviews can be found in the list of references given in the works of Saha et al. from 2019 [7], Grochala from 2018 [8], and Grandinetti from 2018 [2].

The present review is related to the synthetic Ng chemistry of some noble-gas compounds reported in the last five years, with emphasis on the examples reported after 2017, and few studies published before that, which were not mentioned in a 2018 review [2]. Since the present contribution is related to experimental synthesis, pure theoretical papers that predict new Ng compounds are not included. Concerning their number, a separate contribution can be written.

2. Xenon

Chemistry of xenon represents the field with the largest number of synthesized Ng compounds. Xenon(II) fluoride is the only Ng compound that is commercially available and has a wider practical application both in the laboratory use and in the industry. Its main use is in its ability of fluorination of various organic compounds [9,10] and as an etching reagent for surfaces of various metals, oxides, nitrides, etc. [11–16]. It is also used for the preparation of fluorographenes [17–19]. Its applicability for low-temperature insertion of fluorine into oxides systems has been demonstrated with the purpose of modification of magnetic and electronic properties, in particular superconductivity [20]. The ^{18}F labeled XeF_2 is used in nuclear medicine. This includes imaging techniques such as positron emission tomography (PET) as an ^{18}F source [21]. Xenon is shown to bind to other molecules not only under matrix isolation (Lewis acid-base complex of 1,2-azaborine and Xe) [22] but also bulk-phases with metal-xenon bonds have been prepared and their crystal structures determined [23]. In a recent work from surface science, the Xe-Ru interactions with a significant amount of charge transfer were demonstrated at room temperature and low pressures [24]. Using new strategies taking advantage of confinement effects, these new two-dimensional structures allow the study of noble gas metal interactions down to the atomic scale, using the very sensitive toolkit of surface science methodology. The general ideas for using confinement effects for favoring interactions of noble gases with other elements at mild conditions is described in a recent topical review [25].

2.1. Xenon(II)

Since the first reported case of a compound with a XeF_2 ligand coordinated to a metal center, i.e., $[Ag(XeF_2)_2](AsF_6)$ [26], a large number of other examples have been synthesized [27]. A variety of compounds exist, where different numbers of XeF_2 molecules are bound to various metal centers yielding $[M(XeF_2)_x]^{n+}$ cationic part. The oxidation states of the metals are M(I), M(II), or M(III). The most important aspects that influence the formation of XeF_2 coordination compounds are charge and the size of the cation, the type of the anion that compensates the positive charge of the cationic part, solubility of the salt, and the concentration of the XeF_2 ligand [27].

Beside acting as a neutral ligand, XeF_2 acts as a fluoride ion donor forming $[XeF]^+$ salts with strong Lewis acid pentafluorides (MF_5; M = As, Sb, Bi, etc.) [28]. Although the ionic formulations, i.e., $[XeF]^+[MF_6]^-$, implies complete F^- transfer from XeF_2 to the strong Lewis axcid MF_5, in reality the $[XeF]^+$ cation and its anion exists as ion pairs in their salts that interact through Xe–F···M bridges [28]. An excess of XeF_2 oftentimes results in the formation of $[Xe_2F_3]^+$ salts. Oxidation of ruthenium and iridium metal with an excess of XeF_2 in anhydrous HF as a solvent and further crystallization resulted in the crystal growth of $[Xe_2F_3][RuF_6]\cdot XeF_2$, $[Xe_2F_3][RuF_6]$, and $[Xe_2F_3][IrF_6]$ (Figure 1) [29]. Crystal structure determination of $[Xe_2F_3][MF_6]$ (M = Ru, Ir) showed that their structures are isotypic.

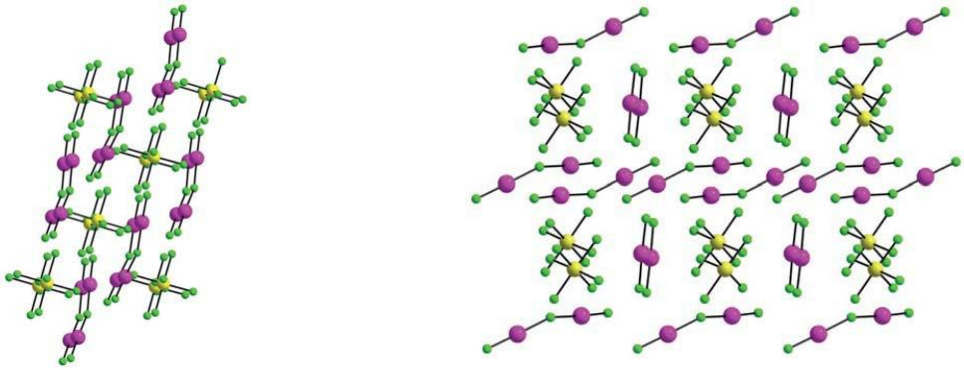

(**a**) (**b**)

Figure 1. (**a**) Packing diagram of $[Xe_2F_3][RuF_6]$ along *b*-axis.; (**b**) Packing diagram of $[Xe_2F_3][RuF_6]\cdot XeF_2$. (reproduced from Ref. [29]; published under the terms and conditions of the Creative Commons Attribution 4.0 International License CC BY 4.0.).

The adducts $XeF_2\cdot CrOF_4$ and $XeF_2\cdot 2CrOF_4$ were synthesized and structurally characterized at low temperatures (Figure 2) [28]. The fluoride ion affinity of $CrOF_4$ is too low to enable fluoride ion transfer from XeF_2 to form ion-paired salts of the $[XeF]^+$ cations having either the $[CrOF_5]^-$ or $[Cr_2O_2F_9]^-$ anions [28].

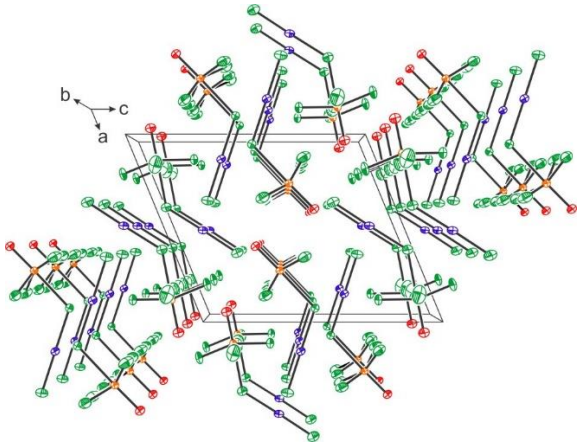

Figure 2. The crystal packing of $XeF_2\cdot CrOF_4$ viewed along the *b*-axis of the unit cell. Copyright (2019) Wiley. Used with permission from Ref. [28].

2.2. Xenon(VI) Fluoride and its $[XeF_5]^+$ and $[Xe_2F_{11}]^+$ Salts

XeF_6 was prepared and isolated in solid argon and neon matrices [30]. The IR spectra of $^{129}XeF_6$ and $^{136}XeF_6$ isotopologues, recorded in the neon matrix, agree with theoretical ones for the C_{3v} conformer of the XeF_6 molecule in the neon matrix. As an internal reference matrix-site and Xe-isotope splitting of corresponding Xe–F and Xe=O stretching modes of $XeOF_4$ were analyzed in solid neon [30].

Xenon hexafluoride is a well-known fluoride ion donor forming various $[XeF_5]^+$ and $[Xe_2F_{11}]^+$ salts [31]. In recent years a large number of crystal structures of previously known or new $[XeF_5]^+$ and $[Xe_2F_{11}]^+$ salts were reported. The crystal structure of $[Xe_2F_{11}][SbF_6]$ consists of $[Xe_2F_{11}]^+$ cations and $[SbF_6]^-$ anions (Figure 3) [32]. The crystal structures of $[XeF_5][SbF_6]$ [33], $[XeF_5][Sb_2F_{11}]$ [33], and $[XeF_5][BF_4]$ [32] are all built from $[XeF_5]^+$ cations (Figure 3). Positive charge of the $[XeF_5]^+$ cations is compensated by $[SbF_6]^-$, $[Sb_2F_{11}]^-$ or $[BF_4]^-$, respectively, anions (Figure 3).

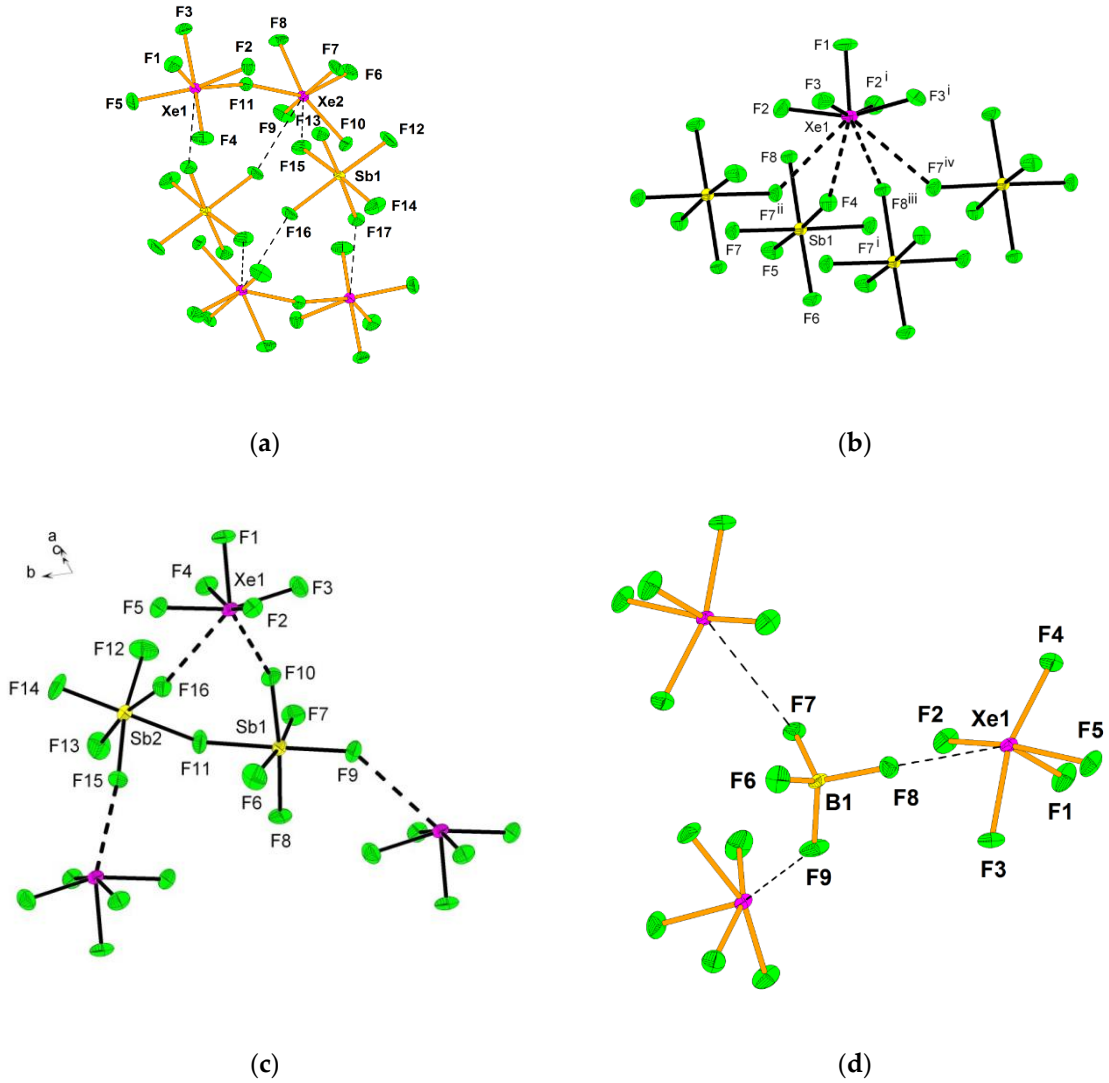

Figure 3. (**a**) Part of the crystal structure of $[Xe_2F_{11}][SbF_6]$. Copyright (2017) Wiley. Used with permission from Ref. [32]; (**b**) Part of the crystal structure of the XeF_5SbF_6 showing the interactions between the $[XeF_5]^+$ cation and the $[SbF_6]^-$ anions. Copyright (2015) Elsevier. Used with permission from Ref. [33]; (**c**) Part of the crystal structure of $XeF_5Sb_2F_{11}$ showing the interactions between the $[Sb_2F_{11}]^-$ anion and the three $[XeF_5]^+$ cations. Copyright (2015) Elsevier. Used with permission from Ref. [33]; (**d**) Part of the crystal structure of $[XeF_5][BF_4]$. Copyright (2017) Wiley. Used with permission from Ref. [32].

Reactions between various amounts of XeF_2 and MF_2, MF_3, or MF_4 (M = Ti, Mn, Sn, Pb) with UV-photolyzed F_2 in liquid anhydrous hydrogen fluoride (aHF) [34] resulted in the crystal growth of a large number of $[XeF_5]^+$ and $[Xe_2F_{11}]^+$ salts upon crystallization from corresponding solutions. Investigation of XeF_2/TiF_4/UV-irradiated system resulted in the crystal structure determinations of $[XeF_5][TiF_5]$ ($XeF_6{\cdot}TiF_4$), $[XeF_5]_5[Ti_{10}F_{45}]$ ($XeF_6{\cdot}2TiF_4$), and $[XeF_5][Ti_3F_{13}]$ ($XeF_6{\cdot}3TiF_4$) [35]. The main structural feature of $[XeF_5][TiF_5]$ is an infinite chain of distorted TiF_6 octahedra joined by cis vertices. Anionic part of $[XeF_5][Ti_3F_{13}]$ is built from tetrameric Ti_4F_{20} and octameric Ti_8F_{36} units sharing vertexes and alternatively linked into $([Ti_3F_{13}]^-)_\infty$ columns. In both cases the charge balance is maintained by $[XeF_5]^+$ cations which form secondary Xe···F contacts with fluorine atoms of anionic parts (Figure 4).

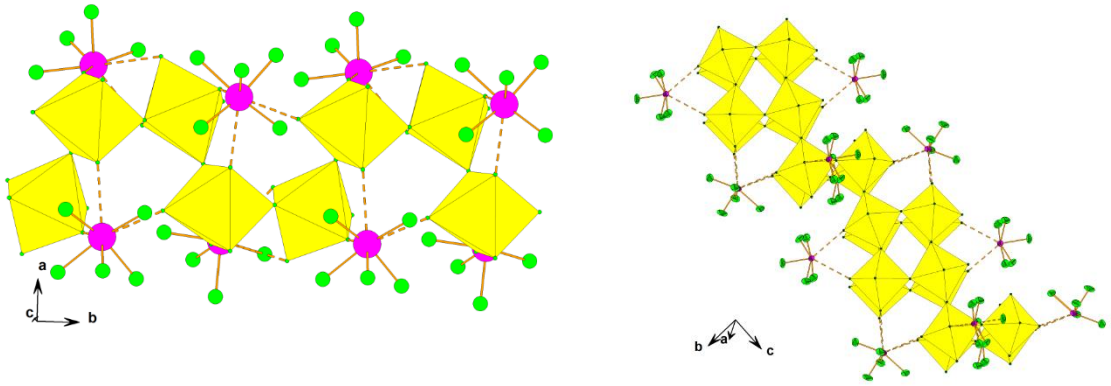

(**a**) (**b**)

Figure 4. (**a**) Part of the $([TiF_5]^-)_\infty$ chain in $[XeF_5][TiF_5]$; (**b**) Part of the infinite $([Ti_3F_{13}]^-)_\infty$ column in $[XeF_5][Ti_3F_{13}]$. Ref. [35]; reproduced by permission of The Royal Society of Chemistry (RSC) on behalf of the Centre National de la Recherche Scientifique (CNRS) and the RSC.

The crystal structure of $[XeF_5]_5[Ti_{10}F_{45}]$ consists of $[XeF_5]^+$ cations and the largest known discrete $[Ti_{10}F_{45}]^{5-}$ anion built from ten TiF_6 octahedra, sharing vertices in the shape of a double-star (Figure 5). It crystallizes in two crystal modification at low (α-phase, 150 K) and ambient (β-phase, 296 K) temperatures.

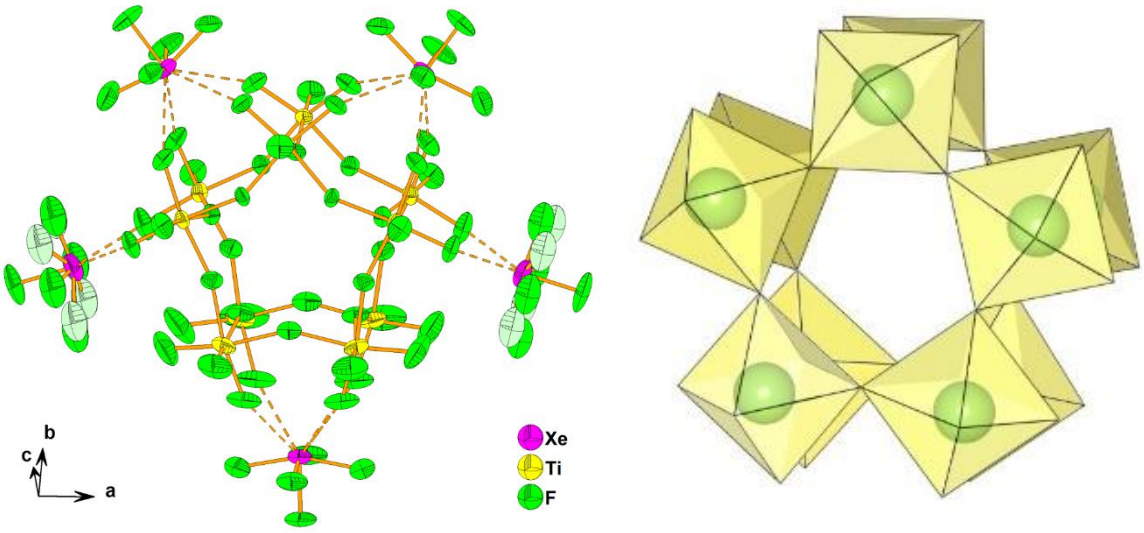

(**a**) (**b**)

Figure 5. (**a**) $[XeF_5]^+$ cations and $[Ti_{10}F_{45}]^{5-}$ anions, composed of ten TiF_6 octahedra, in β-$[XeF_5]_5[Ti_{10}F_{45}]$. Ref. [35]; reproduced by permission of The Royal Society of Chemistry (RSC) on behalf of the Centre National de la Recherche Scientifique (CNRS) and the RSC; (**b**) Geometry of the $[Ti_{10}F_{45}]^{5-}$ anion (Figure was made by Z.M. using crystallographic data from CIF-file of β-$[XeF_5]_5[Ti_{10}F_{45}]$ [35]).

Photochemical synthesis between XeF_2, MnF_3, and UV-irradiated elemental F_2 in aHF yielded $[XeF_5]_2[MnF_6]$ ($2XeF_6{\cdot}MnF_4$), $[XeF_5][MnF_5]$ ($XeF_6{\cdot}MnF_4$) and $[XeF_5]_4[Mn_8F_{36}]$ ($XeF_6{\cdot}2MnF_4$) [36]. The crystal structure of $[XeF_5]_2[MnF_6]$ consists of $[XeF_5]^+$ cations and octahedral $[MnF_6]^{2-}$ anions (Figure 6).

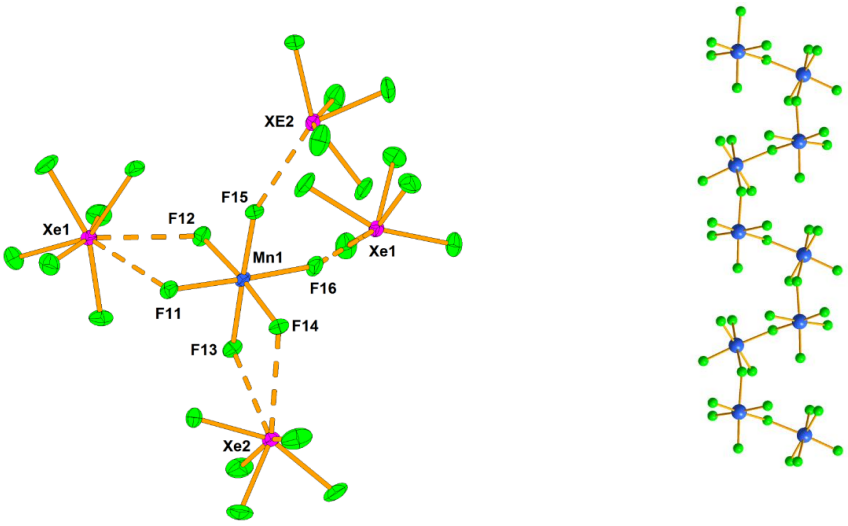

(**a**) (**b**)

Figure 6. (**a**) The secondary contacts between the $[MnF_6]^{2-}$ anion and $[XeF_5]^+$cations in the crystal structure of $[XeF_5]_2[MnF_6]$; (**b**) Part of the $([MnF_5]^-)_\infty$ infinite chain in the crystal structure of $[XeF_5][MnF_5]$. Copyright (2017) Wiley. Used with permission from Ref. [36].

The main structural feature of the anionic part in $[XeF_5][MnF_5]$ is similar to that in $[XeF_5][TiF_5]$ (Figure 4a), although the compounds are not isotypic (Figure 6b). A study of magnetic properties showed that $[XeF_5][MnF_5]$ is paramagnetic in the 296–200 K range (μ_{eff} = 3.87 μ_B, θ = −9.3 K). Below 100 K, there is a weak antiferomagnetic coupling between the Mn(IV) ions (J = −1.3 cm^{-1}) [36].

Crystal structure of $[XeF_5]_4[Mn_8F_{36}]$ consists from $[XeF_5]^+$ cations and discrete $[Mn_8F_{36}]^{4-}$ anions (Figure 7). The latter are built from eight MnF_6 octahedra, each sharing three vertices, in the shape of a ring (Figure 7).

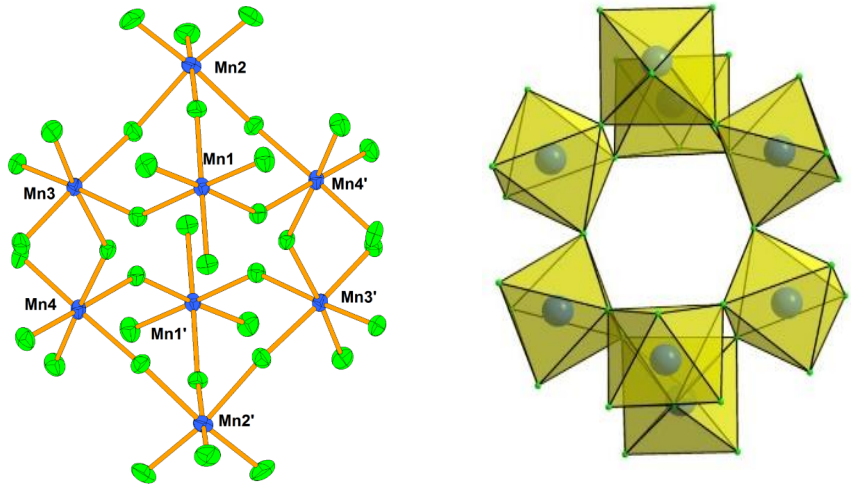

(**a**) (**b**)

Figure 7. (**a**) Discrete octameric $[Mn_8F_{36}]^{4-}$ anion in the crystal structure of $[XeF_5]_4[Mn_8F_{36}]$; (**b**) Geometry of the $[Mn_8F_{36}]^{4-}$ anion built from eight MnF_6 octahedra. Copyright (2017) Wiley. Used with permission from Ref. [36].

The attempts to grow single crystals in XeF_6/MF_4 (M = Sn, Pb) system were successful in three cases. Single crystals of $[Xe_2F_{11}]_2[SnF_6]$, $[Xe_2F_{11}]_2[PbF_6]$, and $[XeF_5]_4[Sn_5F_{24}]$ were grown from aHF saturated

solutions upon crystallizations [37]. The crystal structures of $[Xe_2F_{11}]_2[SnF_6]$ and $[Xe_2F_{11}]_2[PbF_6]$ are isotypic. They consist of $[Xe_2F_{11}]^+$ cations and $[MF_6]^{2-}$ (M = Sn, Pb) anions (Figure 8).

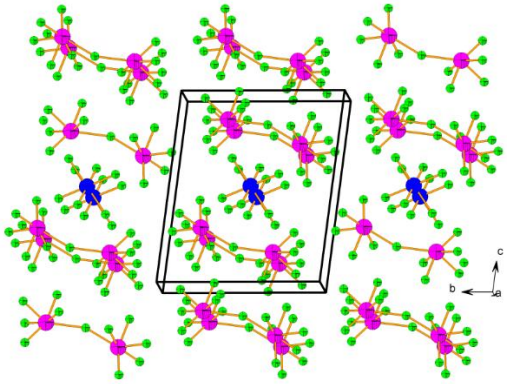

Figure 8. Packing of the $[Xe_2F_{11}]^+$ cations and $[MF_6]^{2-}$ anions in the crystal structures of $[Xe_2F_{11}]_2[MF_6]$ (M = Pb, Sn). Copyright (2019) Wiley. Used with permission from Ref. [37].

The single crystal structure determination of $[XeF_5]_4[Sn_5F_{24}]$ reveals that it is built of two-dimensional $([Sn_5F_{24}]^{4-})_\infty$ grids and the $[XeF_5]^+$ cations located between them. The two-dimensional grids have a wave-like conformation (Figure 9). The $([Sn_5F_{24}]^{4-})_\infty$ layer contains, both six- and seven-coordinated Sn(IV) interconnected by bridging fluorine atoms (Figure 9). It is a unique example of Sn(IV)-fluoride compound that does not consist just of $[SnF_6]^{2-}$ anions. The coordination of Sn(IV) by seven fluorine atoms is unprecedented.

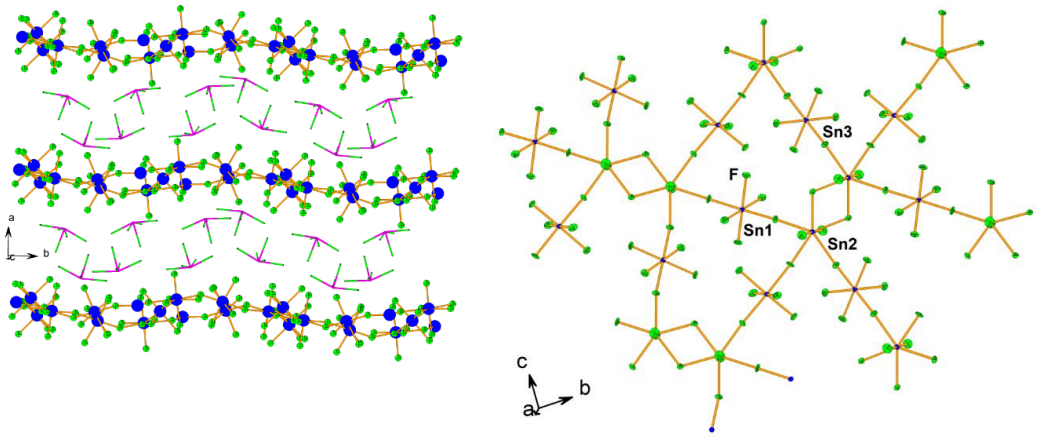

(**a**) (**b**)

Figure 9. (**a**) Two-dimensional $([Sn_5F_{24}]^{4-})_\infty$ grids with a wave-like conformation and the $[XeF_5]^+$ cations located between them in the crystal structure of $[XeF_5]_4[Sn_5F_{24}]$. For clarity, the $[XeF_5]^+$ cations are presented with sticks only; (**b**) The $([Sn_5F_{24}]^{4-})_\infty$ layer in the crystal structure of $[XeF_5]_4[Sn_5F_{24}]$ contains both six- and seven-coordinated Sn(IV) interconnected by bridging fluorine atoms (view perpendicular to the layer, along the *a*-axis). Copyright (2019) Wiley. Used with permission from Ref. [37].

Reactions between molten mixtures of XeF_6 and $Cr^{VI}OF_4$ proceeds by F_2 elimination to form $[XeF_5][Xe_2F_{11}][Cr^{V}OF_5]\cdot 2Cr^{VI}OF_4$, $[XeF_5]_2[Cr^{IV}F_6]\cdot 2Cr^{VI}OF_4$, $[Xe_2F_{11}]_2[Cr^{IV}F_6]$, and $[XeF_5]_2[Cr^{V}{}_2O_2F_8]$ [38]. On the other side, their reactions in aHF and $CFCl_3$/aHF yield $[XeF_5]_2[Cr^{V}{}_2O_2F_8]\cdot 2HF$ and $[XeF_5]_2[Cr^{V}{}_2O_2F_8]\cdot 2XeOF_4$ [38]. Their crystal structures contain $[XeF_5]^+$ and/or $[Xe_2F_{11}]^+$ cations, which interact with their respective anions by secondary Xe···F interactions. In the case of

$[XeF_5][Xe_2F_{11}][Cr^{V}OF_5]\cdot 2Cr^{VI}OF_4$ and $[XeF_5]_2[Cr^{IV}F_6]\cdot 2Cr^{VI}OF_4$, the $CrOF_4$ is introduced into the coordination sphere of $[Cr^{V}OF_5]^{2-}$ and $[Cr^{IV}F_6]^{2-}$ anions, respectively, upon crystallizations (Figure 10). The crystal structure of $[Xe_2F_{11}]_2[Cr^{IV}F_6]$ is comprised of $[Xe_2F_{11}]^{+}$ cations and $[Cr^{IV}F_6]^{2-}$ anions.

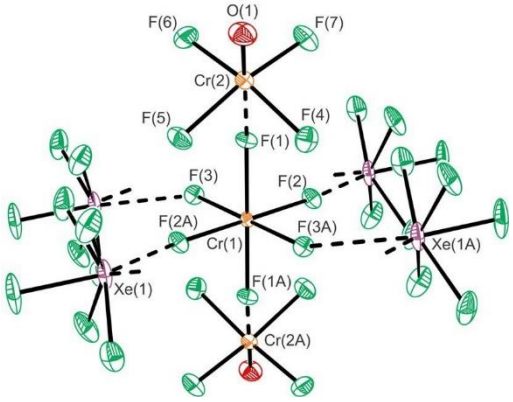

Figure 10. The coordination sphere of the $[CrF_6]^{2-}$ in the crystal structure of $[XeF_5]_2[Cr^{IV}F_6]\cdot 2Cr^{VI}OF_4$. Secondary Xe····F and Cr···F bonding interactions are indicated by dashed lines. Copyright (2019) Wiley. Used with permission from Ref. [38].

The crystal structures of $[XeF_5]_2[Cr^{V}{}_2O_2F_8]$, $[XeF_5]_2[Cr^{V}{}_2O_2F_8]\cdot 2HF$, and $[XeF_5]_2[Cr^{V}{}_2O_2F_8]\cdot 2XeOF_4$ contain $[Cr^{V}{}_2O_2F_8]^{2-}$ anions, where the latter represents a new structural motif among the known oxyfluoroanions of Group 6 (Figure 11) [38].

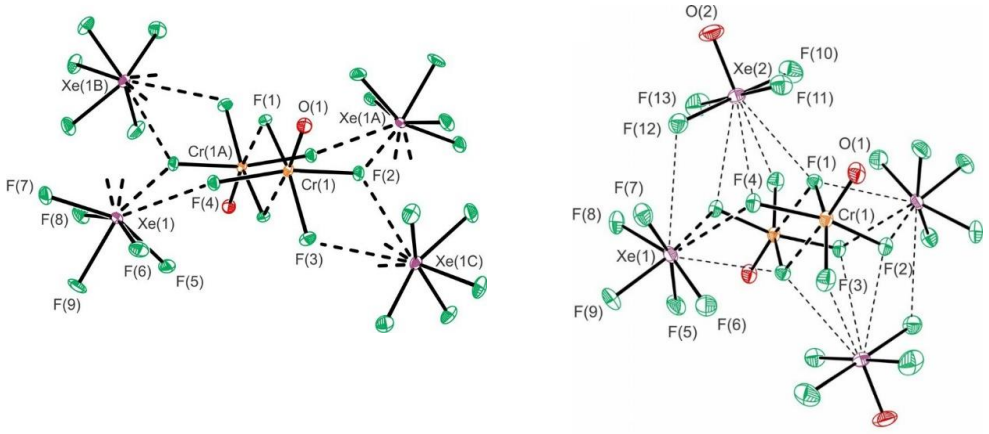

(**a**) (**b**)

Figure 11. (**a**) The coordination sphere of the $[Cr_2O_2F_8]^{2-}$ anion in the crystal structure of $[XeF_5]_2[Cr^{V}{}_2O_2F_8]$. Secondary Xe···F bonding interactions and Cr···F_b bridge bonds are indicated by dashed lines; (**b**) The coordination environment around the $[Cr^{V}{}_2O_2F_8]^{2-}$ anion in the crystal structure of $[XeF_5]_2[Cr^{V}{}_2O_2F_8]\cdot 2XeOF_4$. Secondary Xe···F bonding interactions and Cr···F_b bridge bonds are indicated by dashed lines. Copyright (2019) Wiley. Used with permission from Ref. [38].

Reactions between $ASbF_6$ (A = Rb, Cs) and $[XeF_5][SbF_6]$ in aHF in 1:1 molar ratios yielded $A[XeF_5][SbF_6]_2$ compounds upon crystallization [32]. A similar reaction between $CsBiF_6$ and $[XeF_5][SbF_6]$ (1:1) yielded mixed-cation/mixed-anion $Cs[XeF_5][Bi_xSb_{1-x}F_6]_2$ (x = ~0.37–0.39). The $A[XeF_5][SbF_6]_2$ (A = Rb, Cs) and $Cs[XeF_5][Bi_xSb_{1-x}F_6]_2$ salts crystallize in two crystal modifications at low (α-phase, 150 K) and ambient (β-phase, 296 K) temperatures (Figure 12). High temperature modifications of $A[XeF_5][SbF_6]_2$ (A = Rb, Cs) and $Cs[XeF_5][Bi_xSb_{1-x}F_6]_2$ are structurally related, while low-temperature modifications crystallize isotopically.

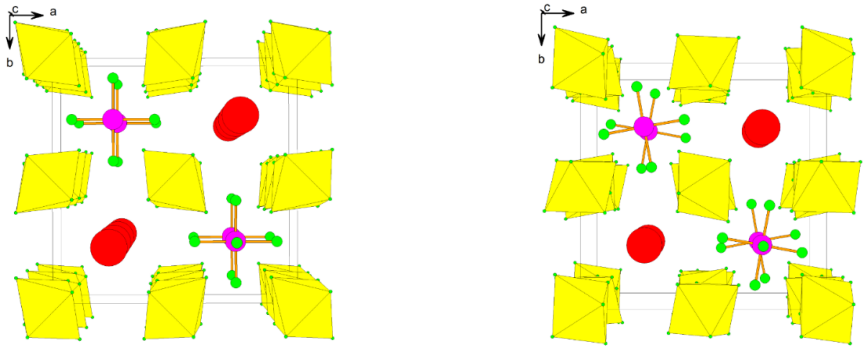

(**a**) (**b**)

Figure 12. (**a**) Packing of Rb^+ and $[XeF_5]^+$ cations and $[SbF_6]^-$ anions in the crystal structure of high-temperature (296 K) form of β-$Rb[XeF_5][SbF_6]_2$; (**b**) Packing of Rb^+ and $[XeF_5]^+$ cations and $[SbF_6]^-$ anions in the crystal structure of low-temperature (150 K) modification of α-$Rb[XeF_5][SbF_6]_2$. Copyright (2017) Wiley. Used with permission from Ref. [32].

Reactions between XeF_5SbF_6 and NO_2SbF_6 or $Cu(SbF_6)_2$, respectively, at ambient temperature in aHF as a solvent yielded the first $[XeF_5]^+$/metal and $[XeF_5]^+$/non-metal mixed-cation salts, i.e., $NO_2XeF_5(SbF_6)_2$ and $XeF_5Cu(SbF_6)_3$ (Figure 13) [39]. Further investigations led to six new examples of such type of compounds, i.e., $XeF_5M(SbF_6)_3$ (M = Ni, Mg, Zn, Co, Mn and Pd) [40]. Additionally, single crystals of $(XeF_5)_3[Hg(HF)]_2(SbF_6)_7$ were grown and crystal structure determined (Figure 14) [40]. For $XeF_5M(SbF_6)_3$ salts, no phase transition was observed for compounds with M^{2+} (M = Ni, Mg, Cu, Zn, Co) that are smaller than Mn^{2+}. The $XeF_5Mn(SbF_6)_3$ and $XeF_5Pd(SbF_6)_3$ crystallize in the low-temperature (Mn at 150 K and Pd at 260 K; α-phase) and high-temperature modifications (296 K; β-phase). The crystal structures of $XeF_5M(SbF_6)_3$ (M = Ni, Mg, Cu, Zn, Co) and α- $XeF_5Mn(SbF_6)_3$ are isotypic. The main feature of their crystal structures is the tri-dimensional framework consisting of the M^{2+} cations interconnected by the SbF_6 octahedra, forming cavities within which the $[XeF_5]^+$ cations are located (Figure 13).

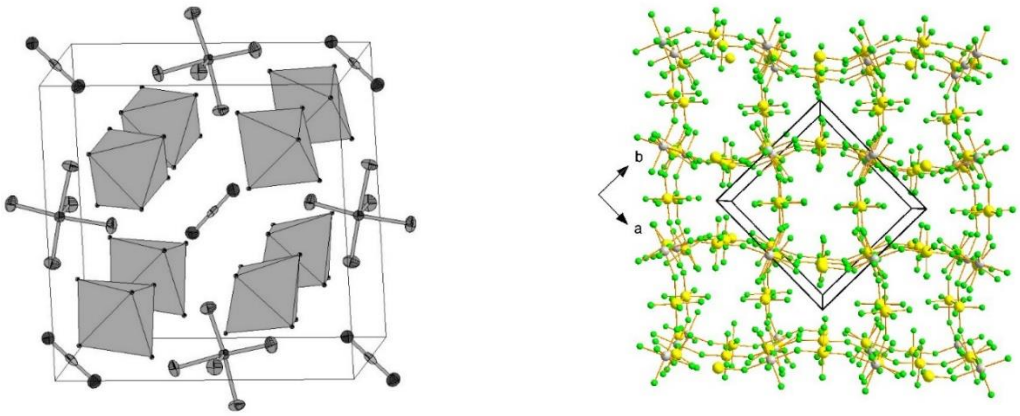

(**a**) (**b**)

Figure 13. (**a**) Packing of $[NO_2]^+$ and $[XeF_5]^+$ cations, and $[SbF_6]^-$ anions in the crystal structure of $NO_2XeF_5(SbF_6)_2$; Only one of the two orientations of the disordered $[SbF_6]^-$ anions is depicted. Copyright (2015) Wiley. Used with permission from Ref. [39]; (**b**) The tri-dimensional $[M(SbF_6)_3]^-$ framework with the monoclinic unit cell in the crystal structure of α-$XeF_5M(SbF_6)_3$ (150 K; M = Mn) isotypic to M^{2+} = Mg, Co, Ni, Zn, and Cu compounds. The $[XeF_5]^+$ cations located within the cavities are omitted for clarity. Copyright (2016) Wiley. Used with permission from Ref. [40].

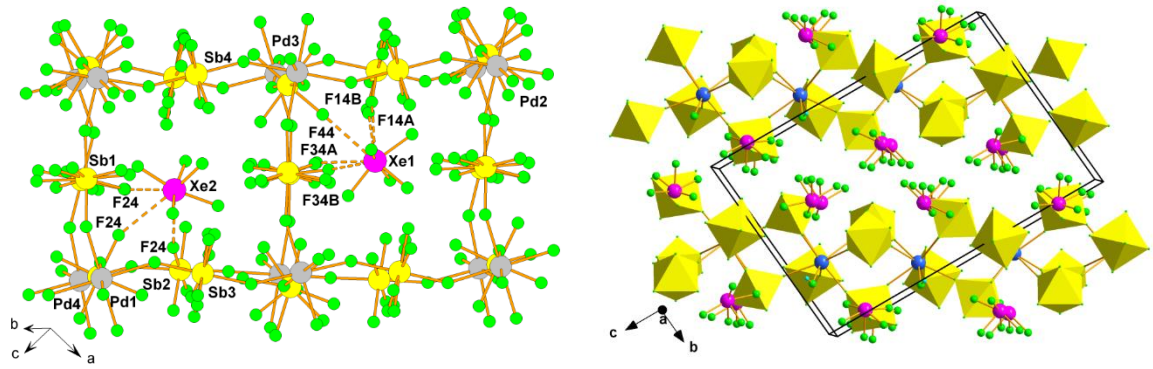

(**a**) (**b**)

Figure 14. (**a**) Part of the crystal structure of β-$XeF_5Pd(SbF_6)_3$ (296 K). Disorder of $[XeF_5]^+$ cations is not depicted. Only F atoms involved in secondary Xe···F contacts are labeled; (**b**) Packing of the columns in the crystal structure of $(XeF_5)_3[Hg(HF)]_2(SbF_6)_7$ with a triclinic unit cell. Copyright (2016) Wiley. Used with permission from Ref. [40].

Although crystal structures of β-$XeF_5Mn(SbF_6)_3$ and α- and β-modifications of $XeF_5Pd(SbF_6)_3$, with larger M^{2+} cations, differ from the other $XeF_5M(SbF_6)_3$ compounds the main structure motif is preserved, i.e., a three-dimensional (3D) framework constructed of the M^{2+} cations and SbF_6 units and $[XeF_5]^+$ cations located inside the cavities (Figure 14).

2.3. Xenon(VI) Oxide Compounds

One of the main obstacles in the research of XeO_3 is its extreme sensitivity. Solid XeO_3 detonates when subjected to mild thermal or mechanical shock. For these reasons, experiments are usually limited to small quantities of XeO_3 and its compounds (up to 20 mg).

The 15-crown adduct of XeO_3, i.e., $(CH_2CH_2O)_5XeO_3$ was synthesized at ambient temperature by reaction of 15-crown-5 with HF-acidified aqueous solution of XeO_3 [41]. It was structurally characterized by Raman spectroscopy and single-crystal X-ray diffraction (Figure 15).

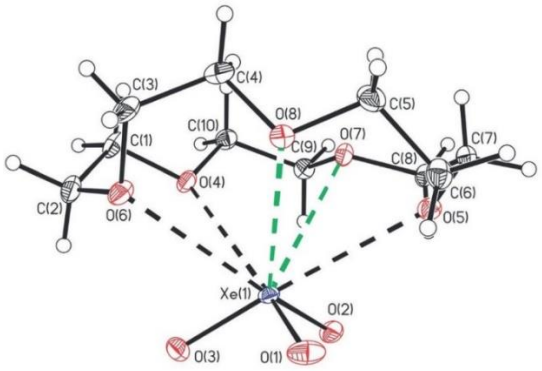

Figure 15. Side-on view of the structural unit in the crystal structure of $(CH_2CH_2O)_5XeO_3$. Copyright (2018) Wiley. Used with permission from Ref. [41].

The crystalline adducts of XeO_3 with triphenylphosphine oxide, dimethylsulfoxide (DMSO), pyridine-N-oxide, and acetonetriphenyl were prepared and characterized by low-temperature, single-crystal X-ray diffraction and Raman spectroscopy [42]. In $[(CH_3)_2CO]_3XeO_3$ each of the XeO_3 molecules is coordinated to three acetone molecules (Figure 16). The structural unit of $[(CH_3)_2SO]_3(XeO_3)_2$ is comprised of three DMSO ligands that bridge two XeO_3 molecules (Figure 16),

whereas in $(C_5H_5NO)_3(XeO_3)_2$ two molecules of XeO_3 are O-bridged by C_5H_5NO ligand and are each O-coordinated to a terminal C_5H_5NO (Figure 16). The $[(C_6H_5)_3PO]_2XeO_3$ (low- and high-temperature modification) provides the only example of a five-coordinate XeO_3 adduct which has only two secondary Xe···O bonding interactions (Figure 16).

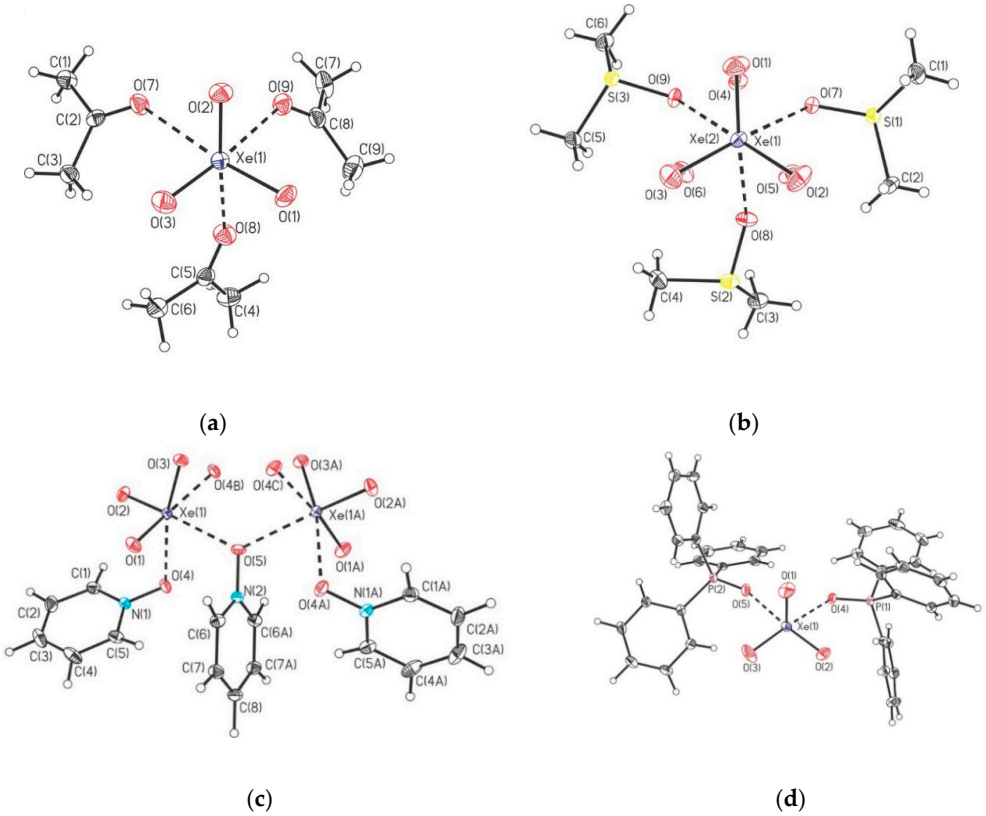

Figure 16. The structural units in the crystal structures of (**a**) $[(CH_3)_2CO]_3XeO_3$; (**b**) $[(CH_3)_2SO]_3(XeO_3)_2$; (**c**) $(C_5H_5NO)_3(XeO_3)_2$; (**d**) $[(C_6H_5)_3PO]_2XeO_3$. Copyright (2019) Wiley. Used with permission from Ref. [42].

Adducts between XeO_3 and N-bases (pyridine and 4-dimethylaminopyridine) were also reported (Figure 17) [43]. Additionally, the crystal structures of the XeO_3 adducts with the fluoride and bifluoride salts of their pyridinium cations were determined (Figure 18) [43].

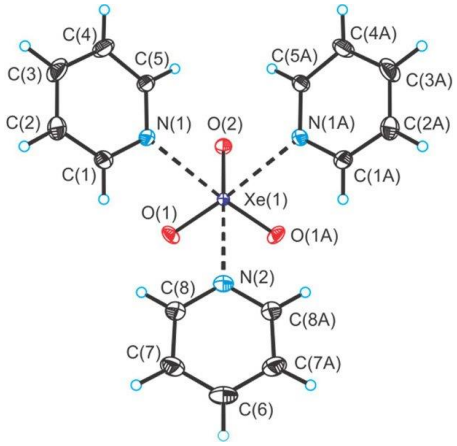

Figure 17. Top-down view of $(C_5H_5N)_3XeO_3$ in the X-ray crystal structure of $(C_5H_5N)_3XeO_3$. Copyright (2018) Elsevier. Used with permission from Ref. [43].

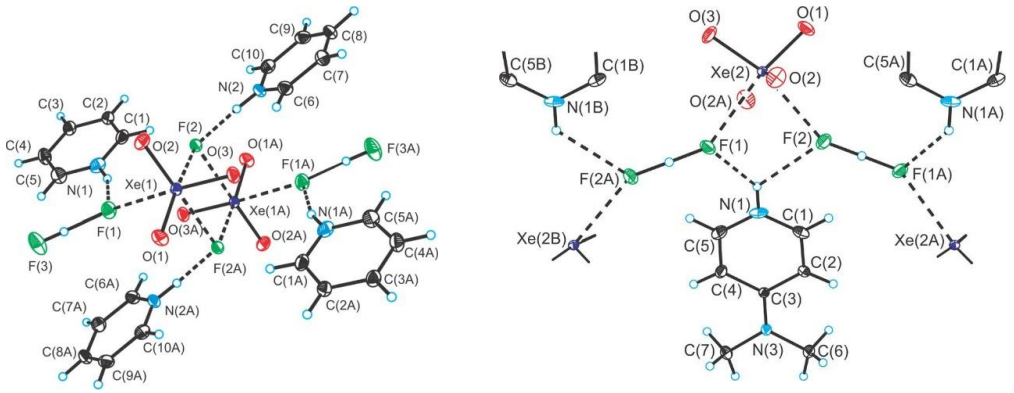

(**a**) (**b**)

Figure 18. (**a**) The X-ray crystal structure of $[C_5H_5NH]_4[HF_2]_2[F]_2(XeO_3)_2$; (**b**) The X-ray crystal structure of $[4\text{-}(CH_3)_2NC_5H_4NH][HF_2]XeO_3$. Copyright (2018) Elsevier. Used with permission from Ref. [43].

3. Krypton

Beside xenon, krypton is the only noble gas where isolable compounds in macroscopic amounts can be prepared [44]. Its chemistry is limited to the +2 oxidation state. Known krypton(II) compounds are less stable than corresponding xenon(II) salts. Compounds in which KrF_2 serves as a ligand towards Lewis centers have been only recently prepared [45]. The latest example is the synthesis and crystal structure determination of $[Hg(KrF_2)_8][AsF_6]_2{\cdot}2HF$ [45]. It is the first homoleptic KrF_2 coordination complex of a metal cation (Figure 19).

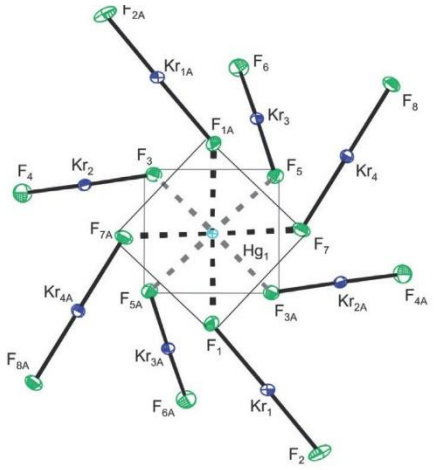

Figure 19. The $[Hg(KrF_2)_8]^{2+}$ cation in the single-crystal X-ray structure of $[Hg(KrF_2)_8][AsF_6]_2{\cdot}2HF$ viewed down the C_2 axis. Copyright (2018) Wiley. Used with permission from Ref. [45].

The $KrF_2{\cdot}CrOF_4$ and $KrF_2{\cdot}2CrOF_4$ adducts were synthesized and their crystal structures determined [28]. The crystal structure of the former comprises of F–Kr–F···Cr(O)F_4 species in which KrF_2 is weakly coordinated to $CrOF_4$ (Figure 20). In the latter both fluorine atoms of KrF_2 coordinate to $CrOF_4$ to form $F_4(O)Cr{\cdots}F–Kr–F{\cdots}Cr(O)F_4$.

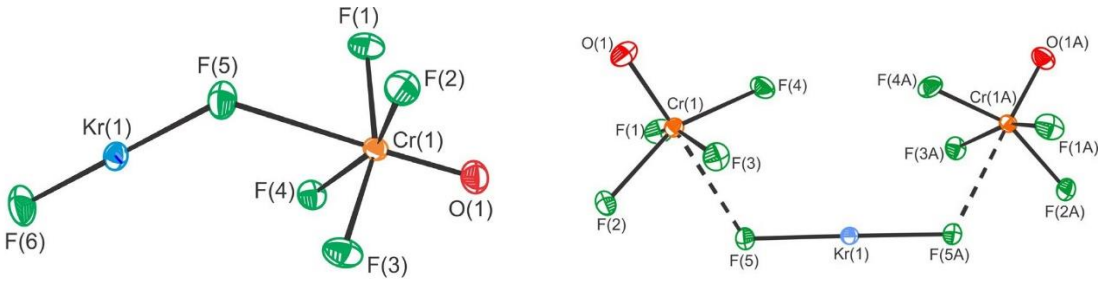

(**a**) (**b**)

Figure 20. (**a**) The X-ray crystal structures of the near-staggered conformation of $KrF_2 \cdot CrOF_4$; (**b**) The structural unit in the X-ray crystal structure of syn-$KrF_2 \cdot 2CrOF_4$. Copyright (2019) Wiley. Used with permission from Ref. [28].

4. Argon, Neon, Helium

In the gas phase all Ng elements including lighter representatives form an exceptionally large family of molecular species, ranging from fragile van der Waals adducts to strongly bound covalent species [2]. Some selected examples from the past include $[Ar–N_2]^+$ [46], $HCCRg^{2+}$ (Rg = Ar and Kr) [47], $ArCF_2^{2+}$ [48] and NeH^+ [49]. ArH^+ was detected in the Crab Nebula, a supernova remnant. It was the first Ng molecule ever found in nature [50]. Charged Ng species, as for example $(XeHXe)^+$, $(KrHKr)^+$, and $(KrHXe)^+$ [51], were synthesized in cold matrix.

4.1. Chemistry of Argon

Experimental chemistry of argon is limited to studies in the low-temperature matrices and molecules observed in the gas phase. The HArF is presently the only experimental known neutral molecule containing a chemically bound argon atom that is stable in a low temperature argon matrix [52]. Another story is the number of reported charged species detected in the gas phase. Some recent examples include observation of $ArCH_2^+$ in mass spectrometry experiments [53] and the production of $ArOH^+$ molecular ion in a pulsed discharge/supersonic expansion of argon seeded with water vapor [54]. The cation complexes $[ArB_3O_4]^+$, $[ArB_3O_5]^+$, $[ArB_4O_6]^+$, and $[ArB_5O_7]^+$ were prepared via laser vaporization supersonic ion source in the gas phase [55]. Superelectophilic fragment anion $[B_{12}(CN)_{11}]^-$, generated from the most stable gas-phase dianion $[B_{12}(CN)_{12}]^{2-}$, binds argon covalently at room temperature [56].

4.2. Chemistry of Neon and Helium

Astrophysical detection of HeH^+ in nearby interstellar space [57] is one of the greatest discoveries in molecular astrophysics. It was the first molecule to form after the big bang [58]. The synthesis of the isolable compounds containing neon and helium still remains an open challenge [8]. In 1992 it was reported that high pressure stabilizes the formation of a solid van der Waals compound of composition $He(N_2)_{11}$, obtained by compression of helium–nitrogen mixtures [59]. A few years ago, the discovery of non-inclusion compound Na_2He at pressures higher than 113 GPa was reported [60]. It was described as an electride, i.e., a crystal made of positively charged ionic cores and with strongly localized valence electrons playing the role of anions. Peculiar Na_2He calls for making our definitions of "compound" more precise [8]. Defect perovskites $(He_{2-x}\square_x)(CaZr)F_6$ can be prepared by inserting helium into $CaZrF_6$ at high pressure [61]. Despite these, helium and also neon have not been forced to form genuine chemical compounds in neutral entities to this day [8]. One of the first steps towards a stable neon compound is claimed to be the experimental observation of the molecular anion $[B_{12}(CN)_{11}Ne]^-$ [62].

5. Bonding Motifs in Noble-Gas Compounds

Despite the inertness of noble gases, Ng chemistry is rich in a variety of species with different bonding motifs [2,4,63]. The bonding motifs are a consequence of the polarization of the spherical electronic cloud of the Ng atoms by binding partners and they range from very weak 'dispersion' to stronger 'induced-dipole' interactions resulting in neutral and ionic 'complexes' of the noble gases, whose character ranges from fragile van der Waals adducts to definitely stable compounds [2].

Clusters of Ng atoms are held together by dispersion forces [2]. In various monocoordinated Ng species [X(Ng)n ($n \geq 1$)], the character of the occurring interactions may span from weakly bound van der Waals adducts, held together by dispersion forces, to strongly bound covalent species [2].

Dicoordinated ('inserted') compounds have a general formula XNgY (X different or the same as Y), the Ng atom being involved in definitely recognizable interactions with both X and Y [2]. They can be neutral or ionic. The bonding of the noble-gas hydrides with the common formula HNgY compounds can be described as $(HNg)^+Y^-$ where $(HNg)^+$ is mainly covalently bonded and the interaction of the $(HNg)^+$ and Y^- is strongly ionic [63]. The most frequently drawn picture of the chemical bonding in XeF_2 is the molecular orbital approach involving three-center, four-electron bonds 3-center 4-electron bonding (3c–4e) [28,64,65]. A single bond is thus spread over the F-Xe-F system.

XeF_2 is a fluoride ion donor and it can form everything from weakly bond complexes to XeF^+ salts with ionic formulation. In the weakly bond complexes [66], the XeF_2 geometry stays intact. In XeF_2 adducts as $XeF_2{\cdot}CrOF_4$ [28] there is a slight elongation of Xe–F_b (F_b = bridging F atom interacting with Cr) bond, while the Xe–F_t (F_t = terminal F atom) bond is slightly shortened [2]. The elongation (weakening) of Xe–F_b and shortening (strengthening) of Xe–F_t bond is observed also in $[M(XeF_2)_x]^{n+}[A]^{n-}$ compounds where XeF_2 is coordinated only by one of its fluorine atoms [27,67]. The distortion of XeF_2 is visible in its Raman spectrum. Its vibrational band at 497 cm^{-1} is replaced by two vibrational bands. One is higher and one lower than 497 cm^{-1} [67]. Numerous products of reactions between XeF_2 and various fluorides are formulated as $[XeF]^+$ salts [28]. Although their formulations imply a simple ionic nature, there is no complete F^- transfer between XeF_2 and fluoride ion acceptor [28]. The $[XeF]^+$ cation and its anion interact through Xe–F···M bridges and the difference between Xe–F_b and Xe–F_t bond lengths is much more pronounced. Structural and vibrational evidences for the ionization pathway $XeF_2 \rightarrow XeF^+ + F^-$ were obtained studying the XeF_2/XeF_5AsF_6 system [68] where at least five distinct well-characterized phases exist in the phase diagram of the XeF_2/XeF_5AsF_6 mixture, and each of them exhibit a more or less pronounced dissociation of XeF_2 into the ionic $[XeF^+]\cdots[A–F^-]$ form (A = Lewis acid) [63].

The bonding in XeF_6 has caused considerable controversy that is not completely resolved [69–71]. The XeF_6 is the strongest fluoride ion donor among XeF_2, XeF_4, and XeF_6. It forms a large number of $[XeF_5]^+$ and $[Xe_2F_{11}]^+$ salts with a variety of Lewis acid fluorides and oxyfluorides [4,5]. The $[XeF_5]^+$ cation geometry may be described in terms of pseudo-octahedral AX_5E VSEPR arrangements of five bond pairs (X) and the lone electron pair (E) around Xe (A) which give rise to a square-pyramidal geometry of Xe and five F atoms [38,72]. Although these compounds are ionic in their nature, the $[XeF_5]^+$ and $[Xe_2F_{11}]^+$ cations are extensively associated with their anions through Xe···F (F belongs to the anion) secondary bonding interactions [73].

In XeO_3 adducts, the xenon-ligand bonds may be described as predominantly electrostatic, (weakly covalent) interactions between the highly electrophilic σ-holes of the xenon atom and the electronegative ligand atom [42].

6. Conclusions

This review shows that noble-gas chemistry is still interesting not just to chemists (at least to some of us) but also to astronomers, geologists, etc. For decades, astronomers have pursued for helium hydride HeH^+, made of the two most common elements in the universe. In the laboratory the ion was discovered in 1925 [74]; however, we had to wait almost 100 years for the confirmation of the existence of HeH^+ in nearby interstellar space [57]. High-pressure and high-temperature (by laser-heating)

study of the possible formation of stable compounds between Ar and Ni at thermodynamic conditions representative of the Earth's core resulted in the formation of ArNi compound (at 140 GPa and 1500 K) [75]. This result implies that the presence of argon in the Earth's core is highly probable [75].

Recent review about the noble-gas/noble-metal chemistry suggests an inflation of such complexes, not only in theory or in microscopic amount in cryogenic situation, but also in large-scale syntheses [76].

Additional stimulation in the noble-gas research represents the discovery of noble gas (or aerogen) bonding [77]. It is a novel type of weak attractive noncovalent interaction [78]. According to IUPAC is defined as the attractive interaction between an electron rich atom or group of atoms and any element of Group-18 acting as electron acceptor [79,80].

Funding: The author acknowledges the financial support from the Slovenian Research Agency (research core funding No. P1–0045; Inorganic Chemistry and Technology).

Acknowledgments: We thank the anonymous reviewers for their constructive comments.

Conflicts of Interest: The author declares no conflict of interest.

References

1. Christe, K.O. A renaissance in noble gas chemistry. *Angew. Chem. Int. Ed.* **2001**, *40*, 1419–1421. [CrossRef]
2. Grandinetti, F. *Noble Gas Chemistry, Structure, Bonding and Gas-Phase Chemistry*, 1st ed.; Wiley-VCH Verlag GmbH & Co. KGaA: Weinheim, Germany, 2018.
3. Haner, J.; Schrobilgen, G.J. The chemistry of xenon(IV). *Chem. Rev.* **2015**, *115*, 1255–1295. [CrossRef]
4. Nabiev, S.S.; Sokolov, V.B.; Chaivanov, B.B. Molecular and crystal structures of noble gas compounds. *Russ. Chem. Rev.* **2014**, *83*, 1135–1180. [CrossRef]
5. Brock, D.S.; Schrobilgen, G.J.; Žemva, B. Noble-Gas Chemistry. In *Comprehensive Inorganic Chemistry II*, 2nd ed.; Reedijk, J., Poeppelmeier, K., Eds.; Elsevier B.V.: Amsterdam, The Netherlands, 2013; Volume 1, pp. 755–822.
6. Hope, E.G. Coordination chemistry of the noble gases and noble gas fluorides. *Coord. Chem. Rev.* **2013**, *257*, 902–909. [CrossRef]
7. Saha, R.; Jana, G.; Pan, S.; Merino, G.; Chattaraj, P.K. How far can one push the noble gases towards bonding? A personal account. *Molecules* **2019**, *24*, 2933. [CrossRef]
8. Grochala, W. On the position of helium and neon in the periodic table of elements. *Found. Chem.* **2018**, *20*, 191–207. [CrossRef]
9. Halpern, D.F.; Tavčar, G.; Tramšek, M. Xenon(II) Fluoride. In *e-EROS Encyclopedia of Reagents for Organic Synthesis*; John Wiley & Sons: Hoboken, NJ, USA, 2017; Available online: https://onlinelibrary.wiley.com/doi/10.1002/047084289X.rx001.pub2 (accessed on 29 June 2020).
10. Campbell, M.G.; Hoover, A.J.; Ritter, T. Transition Metal-Mediated and Metal-Catalyzed Carbon–Fluorine Bond Formation. In *Organometallic Fluorine Chemistry*, 1st ed.; Braun, T., Hughes, R.P., Eds.; Springer: Cham, Switzerland, 2015; pp. 1–54.
11. Xia, D.; Notte, J.; Stern, L.; Goetze, B. Enhancement of XeF_2-assisted gallium ion beam etching of silicon layer and endpoint detection from backside in circuit editing. *J. Vac. Sci. Technol. B* **2015**, *33*, 06F501. [CrossRef]
12. Sarkar, D.; Baboly, M.G.; Elahi, M.M.; Abbas, K.; Butner, J.; Piñon, D.; Ward, T.L.; Hieber, T.; Schuberth, A.; Leseman, Z.C. Determination of etching parameters for pulsed XeF_2 etching of silicon using chamber pressure data. *J. Micromech. Microeng.* **2018**, *28*, 045007. [CrossRef]
13. Murdzek, J.A.; George, S.M. Effect of crystallinity on thermal atomic layer etching of hafnium oxide, zirconium oxide, and hafnium zirconium oxide. *J. Vac. Sci. Technol. A* **2020**, *38*, 022608. [CrossRef]
14. Johnson, N.R.; Hite, J.K.; Mastro, M.A.; Eddy, C.R., Jr.; George, S.M. Thermal atomic layer etching of crystalline GaN using sequential exposures of XeF_2 and BCl_3. *Appl. Phys. Lett.* **2019**, *114*, 243103. [CrossRef]
15. Zhang, R.; Drysdale, D.; Koutsos, V.; Cheung, R. Controlled layer thinning and p-type doping of WSe_2 by vapor XeF_2. *Adv. Funct. Mater.* **2017**, *27*, 1702455. [CrossRef]
16. Alias, M.S.; Yang, Y.; Ng, T.K.; Dursun, I.; Shi, D.; Saidaminov, M.I.; Priante, D.; Bakr, O.M.; Ooi, B.S. Enhanced etching, surface damage recovery, and submicron patterning of hybrid perovskites using a chemically gas-assisted focused-ion beam for subwavelength grating photonic applications. *J. Phys. Chem. Lett.* **2016**, *7*, 137–142. [CrossRef] [PubMed]

17. Bulusheva, L.G.; Okotrub, A.V. Electronic Structure of Fluorinated Graphene. In *New Fluorinated Carbons:Fundamentals and Applications*, 1st ed.; Boltalina, O.V., Nakajima, T., Eds.; Elsevier: Amsterdam, The Netherlands, 2017; pp. 177–213.
18. Copetti, G.; Nunes, E.H.; Soares, G.V.; Radtke, C. Mitigating graphene etching on SiO_2 during fluorination by XeF_2. *Mater. Lett.* **2019**, *252*, 11–14. [CrossRef]
19. Wang, A.; Bok, S.; Mathai, C.J.; Thiruvengadathan, R.; Darr, C.M.; Chen, H.; Zachariah, M.R.; Gangopadhyay, K.; McFarland, J.A.; Maschmann, M.R.; et al. Synthesis, characterization and nanoenergetic utillizations of fluorine, oxygen co-functionalized graphene by one-step XeF_2 exposure. *Combust. Flame* **2020**, *215*, 324–332. [CrossRef]
20. Slater, P.; Driscoll, L. Modification of Magnetic and Electronic Properties, in Particular Superconductivity, by Low Temperature Insertion of Fluorine into Oxides. In *Photonic and Electronic Properties of Fluoride Materials*, 1st ed.; Tressaud, A., Poepelmeier, K., Eds.; Elsevier: Amsterdam, The Netherlands, 2016; pp. 401–421.
21. Preshlock, S.; Tredwell, M.; Gouverneur, V. ^{18}F-labeling of arenes and heteroarenes for applications in positron emission tomography. *Chem. Rev.* **2016**, *116*, 719–766. [CrossRef]
22. Edel, K.; Ishibashi, J.S.A.; Liu, S.-Y.; Bettinger, H.F. Superelectrophilicity of 1,2-azadiborane: Formation of xenon and carbon monoxide adducts. *Angew. Chem. Int. Ed.* **2019**, *58*, 4061–4064. [CrossRef]
23. Seppelt, K. Metal-xenon complexes. *Z. Anorg. Allg. Chem.* **2003**, *629*, 2427–2430. [CrossRef]
24. Zhong, J.-Q.; Wang, M.; Akter, N.; Stacchiola, D.J.; Lu, D.; Boscoboinik, J.A. Room-temperature in vacuo chemisorption of xenon atoms on Ru(0001) under interface confinement. *J. Phys. Chem. C* **2019**, *123*, 13578–13585. [CrossRef]
25. Boscoboinik, J.A. Chemistry in confined space through the eyes of surface science-2D porous materials. *J. Phys. Condens. Matter* **2019**, *31*, 063001. [CrossRef]
26. Hagiwara, R.; Hollander, F.; Maines, C.; Bartlett, N. The crystal structure of $[Ag(XeF_2)_2]AsF_6$ formed in the oxidation of Xe by $AgFAsF_6$. *Eur. J. Solid State Chem.* **1991**, *28*, 855–866.
27. Tavčar, G.; Tramšek, M. XeF_2 as a ligand to a metal center, an interesting filed of noble gas chemistry. *J. Fluorine. Chem.* **2015**, *174*, 14–21. [CrossRef]
28. Mercier, H.P.A.; Breddemann, U.; Brock, D.S.; Bortolus, M.R.; Schrobilgen, G.J. Syntheses, structures and bonding of $NgF_2{\cdot}CrOF_4$, $NgF_2{\cdot}2CrOF_4$ (Ng = Kr, Xe), and $(CrOF_4)_\infty$. *Chem. Eur. J.* **2019**, *25*, 12105–12119. [CrossRef] [PubMed]
29. Tramšek, M.; Goreshnik, E.; Tavčar, G. Oxidation of ruthenium and iridium metal by XeF_2 and crystal structure determination of $[Xe_2F_3][RuF_6]{\cdot}XeF_2$ and $[Xe_2F_3][MF_6]$ (M = Ru, Ir). *Acta Chim. Slov.* **2016**, *63*, 369–375. [CrossRef] [PubMed]
30. Gawrilow, M.; Beckers, H.; Riedel, S.; Cheng, L. Matrix-isolation and quantum-chemical analysis of the C_{3v} conformer of XeF_6, $XeOF_4$, and their acetonitrile adducts. *J. Phys. Chem. A* **2018**, *122*, 119–129. [CrossRef]
31. Atwood, D.A. Noble Gases: Inorganic Chemistry. In *Encyclopedia of Inorganic and Bioinorganic Chemistry*; John Wiley & Sons: Hoboken, NJ, USA, 2011; Available online: https://doi.org/10.1002/9781119951438.eibc0150 (accessed on 29 June 2020).
32. Mazej, Z.; Goreshnik, E. Crystal growth and characterization of the mixed-cation $Rb^+/[XeF_5]^+$ and $Cs^+/[XeF_5]^+$ salts. *Eur. J. Inorg. Chem.* **2017**, *2017*, 2800–2807. [CrossRef]
33. Mazej, Z.; Goreshnik, E.A. Single-crystal structure determination of NO_2SbF_6, XeF_5SbF_6 and $XeF_5Sb_2F_{11}$. *J. Fluorine Chem.* **2015**, *175*, 47–50. [CrossRef]
34. Mazej, Z. Photochemical Syntheses of Fluorides in Liquid Anhydrous Hydrogen Fluoride. In *Modern Synthesis Processes and Reactivity of Fluorinated Compounds*, 1st ed.; Groult, H., Leroux, F., Tressaud, A., Eds.; Elsevier: London, UK, 2017; pp. 587–607.
35. Mazej, Z.; Goreshnik, E.A. Largest perfluorometallate $[Ti_{10}F_{45}]^-$ oligomer and polymeric $([Ti_3F_{13}]^-)_\infty$ and $([TiF_5]^-)_\infty$ anions prepared as $[XeF_5]^+$ salts. *New. J. Chem.* **2016**, *40*, 7320–7325. [CrossRef]
36. Mazej, Z.; Goreshnik, E.; Jagličić, Z.; Filinchuk, Y.; Tumanov, N.; Akslerud, L.G. Photochemical synthesis and characterization of xenon(VI) hexafluoridomanaganates(IV). *Eur. J. Inorg. Chem.* **2017**, *2017*, 2130–2137. [CrossRef]
37. Mazej, Z.; Goreshnik, E. Crystal structures of photochemically prepared $(Xe_2F_{11})_2(MF_6)$ (M = Sn, Pb) and $(XeF_5)_4(Sn_5F_{24})$ containing six- and seven-coordinated tin(IV). *Eur. J. Inorg. Chem.* **2019**, *2019*, 1265–1272. [CrossRef]
38. Goettel, J.T.; Bortolus, M.R.; Stuart, D.G.; Mercier, H.P.A.; Schrobilgen, G.J. Chromium oxide tetrafluoride and its reactions with xenon hexafluoride; the $[XeF_5]^+$ and $[Xe_2F_{11}]^+$ salts of the $[Cr^{VI}OF_5]^-$, $[Cr^{V}OF_5]^{2-}$, $[Cr^{V}{}_2O_2F_8]^{2-}$, and $[Cr^{IV}F_6]^{2-}$ anions. *Chem. Eur. J.* **2019**, *25*, 15815–15829. [CrossRef] [PubMed]

39. Mazej, Z.; Goreshnik, E. $[XeF_5]^+$/metal and $[XeF_5]^+$/non-metal mixed-cation salts of hexafluoridoantimonate(V). *Eur. J. Inorg. Chem.* **2015**, *2015*, 1453–1456. [CrossRef]
40. Mazej, Z.; Goreshnik, E. Influence of the increasing size of the M^{2+} cation on the crystal structures of $XeF_5M(SbF_6)_3$ (M = Ni, Mg, Cu, Zn, Co, Mn, Pd) and $(XeF_5)_3[Hg(HF)_2](SbF_6)_7$. *Eur. J. Inorg. Chem.* **2016**, *2016*, 3356–3364. [CrossRef]
41. Marczenko, K.M.; Mercier, H.P.A.; Schrobilgen, G.J. A stable crown ether complex with a noble-gas compound. *Angew. Chem. Int. Ed.* **2018**, *57*, 12448–12452. [CrossRef] [PubMed]
42. Marczenko, K.M.; Goettel, J.T.; Mercier, H.P.A.; Schrobilgen, G.J. Xenon trioxide adducts of *O*-donor ligands; $[(CH_3)_2CO]_3XeO_3$, $[(CH_3)_2SO]_3(XeO_3)_2$, $(C_2H_5NO)_3(XeO_3)_2$, and $[(C_6H_5)_3PO]_2XeO_3$. *Chem. Eur. J.* **2019**, *25*, 12357–12366. [CrossRef] [PubMed]
43. Goettel, J.T.; Mercier, H.P.A.; Schrobilgen, G.J. XeO_3 as adducts of pyridine, 4-dimethylaminopyriridine, and their pyridinium salts. *J. Fluorine Chem.* **2018**, *211*, 60–69. [CrossRef]
44. Lehmann, J.F.; Mercier, H.P.A.; Schrobilgen, G.J. The chemistry of krypton. *Coord. Chem. Rev.* **2002**, *233–234*, 1–39. [CrossRef]
45. DeBackere, J.R.; Schrobilgen, G.J. A homoleptic KrF_2 complex, $[Hg(KrF_2)_8][AsF_6]_2{\cdot}2HF$. *Angew. Chem. Int. Ed.* **2018**, *57*, 13167–13171. [CrossRef]
46. Linnartz, H.; Verdes, D.; Maier, J.P. Rotationally resolved infrared spectrum of the charge transfer complex $[Ar–N_2]^+$. *Science* **2002**, *297*, 116–1167. [CrossRef]
47. Ascenzi, D.; Tosi, P.; Roithova, J.; Ricketts, C.L.; Schröder, D.; Lockyear, J.F.; Parkes, M.A.; Price, S.D. Generation of the organo-rare gas dications $HCCRg^{2+}$ (Rg = Ar and Kr) in the reaction of acetylene dications with rare gases. *Phys. Chem. Chem. Phys.* **2008**, *10*, 7121–7128. [CrossRef]
48. Lockyear, J.F.; Douglas, K.; Price, S.D.; Karwowska, M.; Fijalkowski, K.J.; Grochala, W.; Remeš, M.; Roithova, J.; Schröeder, D. Generation of the $ArCF_2^{2+}$ dication. *J. Phys. Chem. Lett.* **2010**, *1*, 358–362. [CrossRef]
49. Ram, R.S.; Bernath, P.F. Fourier transform emission spectroscopy of NeH^+. *J. Mol. Spectrosc.* **1985**, *113*, 451–457. [CrossRef]
50. Barlow, M.J.; Swinyard, B.M.; Owen, P.J.; Cernicharo, J.; Gomez, H.L.; Ivison, R.J.; Krause, O.; Lim, T.L.; Matsuura, M.; Olofsson, G.; et al. Detection of a noble gas molecular ion, $^{36}ArH^+$, in the Crab Nebula. *Science* **2013**, *342*, 1343–1344. [CrossRef] [PubMed]
51. Tsuge, M.; Kalinowski, J.; Gerber, R.B.; Lee, Y.-P. Infrared identification of proton-bound rare-gas dimers $(XeHXe)^+$, $(KrHKr)^+$, and $(KrHXe)^+$ and their deuterated species in solid hydrogen. *J. Phys. Chem. A.* **2015**, *119*, 2651–2660. [CrossRef] [PubMed]
52. Kriachtchev, L.; Petterson, M.; Runeberg, N.; Lundell, J.; Räsänen, M. A stable argon compound. *Nature* **2000**, *406*, 874–876. [CrossRef] [PubMed]
53. Fortenberry, R.C.; Ascenzi, D. $ArCH_2^+$: A detectable noble gas molecule. *ChemPhysChem* **2018**, *19*, 3388–3392. [CrossRef] [PubMed]
54. Wagner, J.P.; McDonald II, D.C.; Duncan, M.A. An argon-oxygen covalent bond in the $ArOH^+$ molecular ion. *Angew. Chem. Int. Ed.* **2018**, *57*, 5081–5085. [CrossRef]
55. Jin, J.; Li, W.; Liu, Y.; Wang, G.; Zhou, M. Preparation and characterization of chemically bonded argon-boroxol ring cation complexes. *Chem. Sci.* **2017**, *8*, 6594–6600. [CrossRef]
56. Mayer, M.; van Lessen, V.; Rohdenburg, M.; Hou, G.-L.; Yang, Z.; Exner, R.M.; Aprà, E.; Azov, V.A.; Grabowsky, S.; Xantheas, S.S.; et al. Rational design of an argon- binding superelectrophilic anion. *Proc. Natl. Acad. Sci. USA* **2019**, *116*, 8167–8172. [CrossRef]
57. Güsten, R.; Wiesemeyer, H.; Neufeld, D.; Menten, K.M.; Graf, U.U.; Jacobs, K.; Klein, B.; Ricken, O.; Risacher, C.; Strutzki, J. Astrophysical detection of the helium hydride ion HeH^+. *Nature* **2019**, *568*, 357–360. [CrossRef]
58. Croswell, K. Space is the place for impossible molecules. *Knowable Mag. Annu. Rev.* **2019**. Available online: https://www.knowablemagazine.org/article/physical-world/2019/noble-gas-molecules-in-space (accessed on 29 June 2020). [CrossRef]
59. Vos, W.L.; Finger, L.W.; Hemley, R.J.; Hu, J.Z.; Mao, H.K.; Schouten, J.A. A high-pressure van der Walls compound in solid nitrogen-helium mixtures. *Nature* **1992**, *358*, 46–48. [CrossRef]
60. Dong, X.; Oganov, A.R.; Goncharov, A.F.; Stavrou, E.; Lobanov, S.; Saleh, G.; Qian, G.-R.; Zhu, Q.; Gatti, C.; Deringer, V.L.; et al. A stable compound of helium and sodium at high pressure. *Nat. Chem.* **2017**, *9*, 440–445. [CrossRef] [PubMed]

61. Hester, B.R.; dos Santos, A.M.; Molaison, J.J.; Hancock, J.C.; Wilkinson, A.P. Synthesis of defect perovskites $(He_{2-x}\square_x)(CaZr)F_6$ by inserting helium into the negative thermal expansion material $CaZrF_6$. *J. Amer. Chem. Soc.* **2017**, *139*, 13284–13287. [CrossRef] [PubMed]
62. Mayer, M.; Rohdenburg, M.; van Lessen, V.; Nierstenhöfer, M.C.; Aprà, E.; Grabowsky, S.; Asmis, K.R.; Jenne, C.; Warneke, J. First steps towards a stable neon compound: Observation and bonding analysis of $[B_{12}(CN)_{11}Ne]^-$. *Chem. Comun.* **2020**, *56*, 4591–4594. [CrossRef] [PubMed]
63. Grochala, W.; Khriachtchev, L.; Räsänen, M. Noble-Gas Chemistry. In *Physics and Chemistry at Low Temperatures*; Khriachtchev, L., Ed.; CRC Press: Boca Raton, Florida, USA, 2011; pp. 419–446.
64. Braïda, B.; Hiberty, P.C. The essential role of charge-shift bonding in hypervalent prototype XeF_2. *Nature Chem.* **2013**, *5*, 417–422. [CrossRef] [PubMed]
65. Kurzydłowski, D.; Zaleski-Ejgierd, P.; Grochala, W.; Hoffmann, R. Freezing in resonance structures for better packing: XeF_2 becomes $(XeF^+)(F^-)$ at large compression. *Inorg. Chem.* **2011**, *50*, 3832–3840. [CrossRef] [PubMed]
66. Moran, M.D.; Brock, D.S.; Mercier, H.P.A.; Schrobilgen, G.J. Xe_3OF_3+, a precursor to a noble-gas nitrate; syntheses and structural characterizations of $FXeONO_2$, $XeF_2{\cdot}HNO_3$, and $XeF_2{\cdot}N_2O_4$. *J. Am. Chem. Soc.* **2010**, *132*, 13823–13839. [CrossRef]
67. Tavčar, G.; Tramšek, M.; Bunič, T.; Benkič, P.; Žemva, B. New class of coordination compounds with noble gas fluorides as ligands to metal ions. *J. Fluorine Chem.* **2004**, *125*, 1579–1584.
68. Žemva, B.; Jesih, A.; Templeton, D.H.; Zalkin, A.; Cheetham, A.K.; Bartlett, N. Phases in the system XeF_2/XeF_5AsF_6 and structural and vibrational evidence for the following ionization pathway: $XeF_2 \rightarrow XeF^+ + F^-$. *J. Am. Chem. Soc.* **1987**, *109*, 7420–7427. [CrossRef]
69. Kaupp, M.; van Wüllen, C.; Franke, R.; Schmitz, F.; Kutzelnigg, W. The structure of XeF_6 and of compounds isoelectronic with it. A challenge to computational chemistry and to the qualitative theory of the chemical bond. *J. Am. Chem. Soc.* **1996**, *118*, 11939–11950. [CrossRef]
70. Dixon, D.A.; de Jong, W.A.; Peterson, K.A.; Christe, K.O.; Schrobilgen, G.J. Heats of formation of xenon fluorides and the fluxionality of XeF_6 from high level electronic structure calculations. *J. Am. Chem. Soc.* **2005**, *127*, 8327–8634. [CrossRef] [PubMed]
71. Frenking, G.; Lein, M. Electronic Structure of Main-group Compounds. In *Encyclopedia of Inorganic and Bioinorganic Chemistry*; John Wiley & Sons: Hoboken, NJ, USA, 2011; Available online: https://doi.org/10.1002/9781119951438.eibc0067 (accessed on 6 June 2020).
72. Gillespie, R.J.; Hargittai, I. *The VSEPR Model of Molecular Geometry*, 1st ed.; Allyn and Bacon: Boston, MA, USA, 1991.
73. Hughes, M.J.; Mercier, H.P.A.; Schrobilgen, G.J. Syntheses, Raman spectra and X-ray crystal structures of $[XeF_5][\mu\text{-}F(OsO_3F_2)_2]$ and $[M][OsO_3F_3]$ ($M = XeF_5^+$, $Xe_2F_{11}^+$). *Inorg. Chem.* **2010**, *49*, 3501–3515. [CrossRef] [PubMed]
74. Hogness, T.R.; Lunn, E.G. The ionization of hydrogen by electron impact as interpreted by positive ray analysis. *Phys. Rev.* **1925**, *26*, 44–55. [CrossRef]
75. Adeleke, A.A.; Kunz, M.; Greenberg, E.; Prakapenka, V.B.; Yao, Y.; Stavrou, E. A high-pressure compound of argon and nickel: Noble gas in the Earth's core? *ACS Earth Space Chem.* **2019**, *3*, 2517–2524. [CrossRef]
76. Pan, S.; Jana, G.; Merino, G.; Chattaraj, P.K. Noble-noble strong union: Gold at its best to make a bond with a noble gas atom. *ChemistryOpen* **2019**, *8*, 173–187. [CrossRef]
77. Bauzá, A.; Frontera, A. Aerogen Bonding Interaction: A New Supramolecular Force? *Angew. Chem. Int. Ed.* **2015**, *54*, 7340–7343. [CrossRef]
78. Gomila, R.M.; Frontera, A. Covalent and non-covalent noble gas bonding interactions in XeF_n derivatives (n = 2-6): A combined theoretical and ICSD analysis. *Front. Chem.* **2020**, *8*, 395. [CrossRef]
79. Britvin, S.N. Xenon in oxide frameworks: At the crossroads between inorganic chemistry and planetary science. *Dalton Trans.* **2020**, *49*, 5778–5782. [CrossRef]
80. Bauzá, A.; Frontera, A. σ/π hole noble gas bonding interactions: Insights from theory and experiment. *Coord. Chem. Rev.* **2020**, *404*, 213112. [CrossRef]